Qeios

Backstepping Control Design in Conjunction with an EKF-based Sensorless Field-Oriented Control of an IPMSM

Caglar Uyulan[1]

[1]İzmir Katip Çelebi University, Faculty of Engineering and Architecture, Department of Mechanical Engineering, İzmir, Turkey

ORCID and email: 0000-0002-6423-6720 / caglar.uyulan@ikcu.edu.tr

Abstract

The collector and brushless electronic commutation machines have gained widespread utilization in industrial applications. Among these machines, internal permanent magnet synchronous motors (IPMSMs) have become increasingly popular due to their numerous advantages, including high torque/current and torque/inertia ratios, robust construction, high efficiency, and reliability. However, the incorporation of position sensors in IPMSMs has introduced challenges concerning their application, performance, mass production, and cost. Consequently, the implementation of sensorless control techniques has become essential in drive systems and various applications.

This paper proposes a backstepping control approach for achieving speed sensorless control of IPMSMs, employing an extended Kalman filter (EKF). The first step involves developing a comprehensive nonlinear dynamical model of the IPMSM in the direct and quadrature (d-q) rotor frame and obtaining its corresponding state-space representation. Subsequently, backstepping controllers for rotor speed and current tracking are designed to ensure precise tracking and anti-disturbance performance. These controllers are integrated into the field-oriented control (FOC) scheme. The Lyapunov stability theorem is employed to guarantee the asymptotic stability condition of the backstepping controller.

To address the challenge of estimating immeasurable mechanical parameters of the IPMSM and accurately tracking the system states, an EKF is designed. This filter enables the estimation of mechanical parameters and achieves high steady-state precision within a finite time. The effectiveness of the proposed methodology is demonstrated through simulations conducted under various dynamic operating conditions, including sudden torque load changes, command speed changes, and parameter variations.

Keywords: Sensorless field oriented control, internal permanent magnet synchronous motor, electric motor control, backstepping control, extended Kalman filter.

https://doi.org/10.32388/IXUSW5

1. Introduction

Permanent magnet synchronous motors (PMSMs) are electric machines that convert energy by generating torque through the interaction between stator currents and the magnetic field of permanent magnets on the rotor. Unlike brushed DC machines, PMSMs achieve commutation electronically through power electronic switches in the inverter, altering the current direction in the stator windings with each pole change of the rotor magnet. As a result, these electronically commutated machines eliminate the need for a collector and brush assembly. PMSMs can be categorized as trapezoidal (square wave excitation) or sinusoidal (sine wave excitation) based on the shape of the induced voltage in their windings. A sinusoidal brushless direct current motor is commonly referred to as a PMSM [1, 2].

Free-excited direct current motors have remained unrivaled for a long time in the variable speed control systems class, which are widely used in the industry, due to their easy speed control and linear control structure. This is because the current components that make up the flux and the torque can be controlled independently of each other. In this way, when the flux is kept constant, the torque can be controlled linearly with the current component that creates it. Changing the excitation current makes the torque response of the motor slow, but changing the armature current makes the torque response of the motor fast. Therefore, armature current is used to control the torque taken from the motor shaft. The excitation current control, on the other hand, is controlled to go higher than the rated speed. However, the brush commutator structure, which is the biggest disadvantage of these machines, caused the machine to require maintenance at certain intervals and not to be used in flammable and dusty environments. Considering all these disadvantages, variable speed drive systems are used in alternating current machines such as asynchronous motors and PMSMs, which do not have a brush commutator structure instead of a direct current machine. Synchronous motors are double-excited machines that always rotate at a synchronous speed depending on the frequency of the source and the number of poles of the motor. The stators of these motors are fed with alternating current and the rotors with direct current. However, in synchronous motors, when the rotor magnetic field is provided with permanent magnets placed on the rotor, the need for a second source is eliminated and PMSMs are obtained. Instead of brush and collector assembly, electronic drivers are used to provide commutation. The position sensors enable the driver to feed appropriate windings. Since there is no current in the rotor of the motor, there are no rotor copper losses. In addition, the disappearance of the magnetizing current increases the power coefficient of the motor. Therefore, it is possible to design these motors with the same power but smaller dimensions

and higher efficiency than other motors. Excitation with a permanent magnet has provided great advantages to the synchronous motor [3, 4].

If these advantages are listed: the utilization of stator current is solely dedicated to generating torque. As this current lacks a magnetization component, its efficiency surpasses that of an induction motor with equivalent power. Periodic maintenance is unnecessary for these motors as they lack brushes and rings. Consequently, their efficiency increases since there is no heat loss in the rotor. Additionally, they operate more quietly as there is no noise emanating from brushes and collectors. Incorporating a permanent magnet for excitation adds a level of flexibility to motor design. The absence of winding in the rotor results in reduced rotor size, leading to a higher torque/inertia ratio and power ratio. Hence, these motors are particularly favored in applications demanding superior performance, such as robotics and space applications [5].

The d-q axis model applies to permanent magnet synchronous motors (PMSMs), enabling them to be controlled like DC motors. This characteristic makes PMSM motors a compelling alternative to traditional DC motors. For smooth and vibration-free continuous torque generation, the voltage and current excitation must exhibit pure sinusoidal characteristics. In PMSMs, the stator windings surrounding the air gap are distributed sinusoidally, while the magnetic flux density generated by the magnets in the rotor changes along the air gap [6]. The angular position of the rotor at any given time "t" synchronizes with the sinusoidal phase currents supplied to the stator. PMSMs are typically powered by a current-controlled inverter, which relies on current sensors placed on each phase and a high-sensitivity position sensor. Any disturbance that deviates from the phase currents or induced voltage from their sinusoidal waveform will introduce undesired torque vibration components in these motors. Therefore, high-sensitivity optical encoders or angle detectors, such as resolvers, are employed for precise position detection. However, the utilization of such sensors increases the overall cost and complexity of the control system [7, 8].

Permanent magnet synchronous motors (PMSMs) can be classified into two categories: surface magnet machines and internal magnet machines. Surface magnet machines feature a small rotor radius and low inertia torque. The magnetic permeability of magnets in these machines is similar to that of air, resulting in an effective air gap that comprises the actual air gap and the magnet thickness. Since the d-axis and q-axis inductances are equal, surface magnet machines

do not generate reluctance torque. They are prone to demagnetization due to the armature reaction of magnets and are not suitable for field weakening.

On the other hand, internal magnet machines possess a robust mechanical structure as the magnets are positioned inside the rotor. PMSMs with internal magnet structures can generate higher torque per unit volume due to the combined torque contribution from the magnets and armature current. Additionally, reluctance torque is produced due to the differing inductances in the d-axis and q-axis. The magnitude of reluctance torque can be controlled by adjusting the number, thickness, and location of the rotor flux barriers. These machines are widely utilized in industrial applications as ideal electrical machines due to their numerous advantageous features, including high efficiency, compact size, lightweight, the presence of reluctance torque, and a large field weakening range. In the internal magnet structure, the effective air gap is small, making it challenging to demagnetize the magnets [9, 10].

In PMSMs, the constant power-speed range is determined by the structure of the permanent magnet rotor, and optimizing the rotor design can enhance this range. The magnets can be arranged superficially on the rotor, on the inner surface of the rotor, in the form of rods, or as single and multiple barriers. They can also be configured as axial laminations, segmented structures, or in V-shaped or W-shaped arrangements. These arrangements provide exceptionally high inductance values and increase the field weakening capability of the motor [11, 12].

Various techniques have been developed to achieve sensorless control of rotor position and speed in PMSMs, eliminating the need for dedicated sensors. These methods typically involve manipulating motor equations to establish a relationship between terminal values and rotor position/speed. The fundamental principle of sensorless control in PMSMs involves obtaining position information through the analysis of terminal and induced voltage in the motor, which depends on the rotor speed and position; utilization of motor parameters; real-time monitoring and calculation of inductance based on the current; Injection of a high-frequency and low-energy signal to the stator windings; Detection of the two-phase current and conversion of their absolute values into direct current (DC) information; Application of model references adaptive systems to extract position information; Implementation of observer-based techniques or flux estimation algorithms, among others [13-16]. These techniques enable the estimation of rotor position and speed without relying on additional sensors, providing a sensorless approach to control PMSMs.

Sensorless control methods for PMSMs can be categorized into three main groups: model-based state predictors (both adaptive and non-adaptive methods), saliency and signal injection-based methods, and artificial intelligence algorithms. Each method has its advantages and disadvantages. The key criteria for evaluating the superiority of a sensorless position and velocity estimation method include steady-state error, dynamic behavior, noise sensitivity, performance at low speeds, sensitivity to motor parameters, simplicity, response speed, and computational time. Current model-based estimation algorithms are commonly employed in various industries, particularly in-home appliance applications, due to their ease of implementation and robustness against load torque variations. These algorithms estimate the position by comparing the d-axis and q-axis current errors between the actual motor and the predictor model. The accuracy of the motor model parameters plays a crucial role in the effectiveness of this method [17, 18].

In conventional methods, estimation algorithms are utilized to monitor stator voltages and currents. These methods offer several notable advantages, including computational simplicity, minimal observer requirements, and prompt response without any delays. However, achieving high accuracy in motor parameter estimation is crucial, and the susceptibility of these parameters to noise can lead to calculation errors [19-21].

Flux estimation algorithms involve estimating the flux based on voltage and current measurements, which are then used to determine the position through a quadratic polynomial-based curve. To enable sensorless control, it is necessary to start the motor from a known initial position. Consequently, acquiring the initial rotor position information becomes critical for accurate estimation. The main challenges associated with these algorithms include integration errors at low speeds, lengthy computation time, sensitivity to parameter variations, and the requirement of a costly signal processor to solve complex algorithms. Various studies have been conducted to determine the rotor position throughout the entire speed range by utilizing functions based on measured currents and calculated voltages [22-24].

Other studies in the literature have explored flux estimation algorithms as well. One approach involves utilizing active flux monitors, which transform any permanent magnet synchronous machine (PMSM) into a salient pole machine. These monitors incorporate an imaginary flux that accounts for the reluctance torque resulting from the rotor's saliency. By adding this imaginary flux to the magnet's flux, an augmented flux is obtained. Consequently, this augmented flux can be interpreted as a torque-producing flux in salient pole machines, and it

aligns with the transverse axis. This approach improves rotor position and speed estimation accuracy across a wide range of speeds, resulting in reduced dynamic errors [25-26].

In another study, an "active flux" observer and space vector modulation direct torque and flux control were employed for an interior permanent magnet synchronous machine (IPMSM) without the use of a motion sensor or signal injection [27]. The study incorporates a reactance function along the longitudinal axis that accounts for magnetic saturation. Since the effective flux position aligns with the rotor position, this simplification facilitates a more accurate estimation of rotor position and velocity. Field weakening techniques enable the extension of this approach to even higher speeds.

Additionally, a sensorless speed estimation algorithm was developed and analyzed using vector control, based on flux and instantaneous reactive power. However, it is important to note that measurement errors in motor parameters, line currents, and input voltages can introduce inaccuracies in speed estimation [28].

To compensate for errors, the use of instantaneous reactive flux can be employed. This estimation method, based on instantaneous flux, offers superior performance compared to traditional flux estimation methods, as it avoids the issue of thermal drift. The flux-dependent speed estimation relies on the relationship between current and velocity in the α-β axes. By extracting velocity estimates from the voltage equations, which contain velocity information within the induced motion voltage, algorithms can be tested through simulations using a space vector pulse width modulated inverter. This estimation method exhibits lower sensitivity to noise, provides stable information from stator currents and voltages, and achieves higher overall performance.

Sensorless control methods that measure the motion voltage induced in the motor are the simplest and most widely used. Various research studies have been conducted in this area. The sensed electromotive forces (EMFs) are utilized in different ways to determine appropriate switching sequences for the power switch elements in the inverter. However, a major drawback of this method is its inability to accurately perform sensing during start-up especially at low speeds, due to the low induced voltage. Consequently, an additional take-off method is required to apply this technique. As a result, these methods encounter difficulties during take-off and transient operations and are typically applicable only within a narrow speed range. The presence of an artificial neutral point, voltage divider, and filter are notable limitations of these methods. Additionally, at low speeds, position estimation becomes highly sensitive to stator resistance.

Another approach involves using the third harmonic component in the voltage induced in the non-powered phase of permanent magnet synchronous machines (PMSMs) for sensorless control algorithms, including in the field weakening region. This method yields good starting performance, a high torque/current ratio, and high efficiency across a wide speed and load range. However, it faces challenges at low speeds, as the amplitude of the third harmonic component is too small to be reliably detected. Moreover, an additional circuit is often necessary, and position errors can occur during integration at low speeds [29-31].

The induced motion voltage-based methods employ estimation techniques that operate at a frequency equal to the fundamental electrical frequency, which is proportional to the rotational speed of the rotor. The basic analytical torque equations of the motor include current and speed as state variables, making these equations nonlinear. As the speed and position information of the motor exhibit nonlinear behavior, a nonlinear observer is required to accurately perceive them. Initially, these methods were proposed for surface magnet machines, which lack protrusions, making position and velocity information solely reliant on the induced motion voltage. However, in internal magnet synchronous motors, both position information and phase inductance information are influenced by saliency, which refers to the variation in phase inductances based on position. Salient pole synchronous motors, for example, exhibit different inductances in the direct and quadrature axes. By combining an induced motion voltage estimator with the current-based model of the permanent magnet synchronous machine (PMSM), control and position detection issues encountered at low speeds can be resolved [32].

Although accurate estimation of induced motion voltage is achievable, control in low-speed regions remains limited. The induced motion voltage constant varies with different loads and speeds, making accurate prediction challenging. On the other hand, model-based sensorless methods demonstrate robustness in torque control across a wide range of PMSMs. These methods rely on measuring phase currents and voltages and utilizing the motor model for position and velocity estimation, leading to significantly improved accuracy by reducing position errors [33]. To enhance the dynamic performance of traditional induced motion voltage and position sensing methods, the use of a phase-locked loop (PLL), which can introduce system imbalances, is eliminated [34]. Instead of directly filtering the rapidly changing rotor position signal, a high-accuracy starting position is determined by filtering slowly changing signals.

In adaptive methods, the estimated output information is generated by employing real system measurements as input values in the mathematical model of the machine. The discrepancy between the measured quantities and the estimated output information is utilized as feedback in the system model to validate the predicted quantities. The primary advantage of using an observer is the ability to predict all state variables in the system model. However, these methods encounter challenges at low speeds, involve complex algorithms, and require significant computational resources [35].

The extended Luenberger observer (ELO) is well-suited for position and speed estimation in PMSMs due to the nonlinear nature of the PMSM model. In this approach, the nonlinear system model is linearized at each sampling time using the Jacobian matrix. Previous studies have utilized the extended Luenberger observer for state estimation in AC drives [36, 37]. Another adaptive method is model-based adaptive control (MRAC), where the speed and position estimation methods employed can be categorized based on the state variables. Commonly used methods include rotor flux-based, reverse EMF-based, and stator current-based approaches [38, 39]. The extended induced voltage is utilized as a new state variable in adaptive velocity observers [40]. The extended induced voltage encompasses the induced action voltage and the change in phase inductances. By rewriting the motor equations in terms of the extended induced motion voltage, only the position-dependent terms remain in the equation. The position of the internal magnet synchronous motor can be estimated using an expanded induced voltage error observer based on the stator and rotor reference system [41].

In another study, a simplified mathematical model of a PMSM and model reference adaptive control (MRAC) based on voltage and current models were utilized for speed estimation [42]. The model was developed to minimize the effects of MRAC parameter uncertainties and enhance estimation performance. Experimental results showed improved speed response and performance at both low and high speeds. PMSM control using field-oriented control (FOC) methods has also been investigated [43, 44]. A model reference adaptive system (MRAS) was employed to eliminate the need for a speed sensor. The proposed method was tested under balanced and unbalanced motor operating conditions. Luenberger observer-based prediction algorithms generally outperformed MRAS-based systems, which exhibited higher errors in predicted values. Luenberger's approaches require less memory and computation time.

In another study, an extended Kalman filter (EKF) was employed to mitigate problems arising from parameter errors. The EKF method is widely used in nonlinear systems due to its optimality, processing ease, and robustness against parameter changes [45, 46]. With advancements in digital signal processing, the computational time load of the EKF can be easily overcome, allowing for quick implementation using an inexpensive DSP motor controller [47, 48]. The EKF method considers parameter errors and measurement noise in its structure, resulting in high resistance to parameter errors and noise. Since it does not require initial position information for start-up, the motor can be initiated from any unknown initial position [49-52].

Signal injection-based methods utilize changes in inductance in the PMSM relative to the rotor position. A high-frequency voltage or current is injected into the fundamental component, and rotor position information is extracted from current harmonics using signal processing. These methods allow for position information to be obtained during start-up and at low speeds, and they exhibit robustness against parameter changes, providing advantages over other techniques. They can be categorized as rotating injection methods and pulsating injection methods based on the direction of the injected signal. In the literature, there are also methods based on PWM-excited signal processing without signal injection [53, 54]. The estimated position information is obtained by injecting a high-frequency signal into the system, covering a wide range from standstill to high-speed states. One significant advantage of this method is its applicability in a wide range of speeds, from high speeds to zero-speed situations. Rotor position estimation is achieved by applying a high-frequency current signal to the stator windings. Additionally, an adaptive PMSM model is employed, taking into account the variation of machine parameters [55, 56]. Two different sensorless vector control methods were investigated for PMSMs operating in the low-speed range. Various experiments were conducted by adding high and low-frequency signals to the system. According to experimental results, both methods can be easily configured and exhibit efficient operation. While the high-frequency signal addition method yields better dynamic performance, it also introduces higher levels of noise. Methods based on the magnetic saliency effect are complex to implement in real time and are challenging to apply to machines with different structures and features. However, they perform well at low speeds and can be used during start-up [57-59]. A non-linear PMSM model is considered, and the rotor position is determined using the saliency effect. The offsets reflect changes in stator winding inductance based on rotor position and stator phase current. The non-linear inductance of the PMSM is measured at various rotor positions and stator currents. Rotor position and stator

current equations are expressed using the Fourier series. Simulations conducted in low and high-speed regions demonstrated that this method is not suitable for operation in low-speed regions [60].

Artificial neural networks (ANNs), fuzzy logic algorithms, and ANFIS (adaptive neuro-fuzzy inference systems) are artificial intelligence methods employed in the sensorless control of PMSMs. The selection of the network structure and calculation of the control algorithm can be complex, and the trial and error system in the ANN structure makes the applicability of sensorless control challenging, reducing its reliability and increasing the error rate [61-63]. In one study, a high-frequency low voltage was applied to the stator to determine the initial rotor position using an artificial neural network. The currents flowing through the stator phases and the rotor position at that moment were recorded by applying voltages. This process was repeated for different rotor positions, creating a learning set for the artificial neural network. During operation, the motor was first energized with test voltages, and the measured currents were applied to the ANNs to determine the instantaneous initial rotor position. The study observed minimal position error after experimentation [64].

This study aims to employ a robust sensorless control algorithm that can operate effectively across a wide range of speeds and variable load profiles. To achieve this goal, the backstepping control algorithm based on the extended Kalman filter (EKF) is utilized due to its computational efficiency and accuracy. The remaining sections of this paper are organized as follows. In Section 2, the mathematical model of the interior permanent magnet synchronous motor (IPMSM) is presented. Section 3 introduces the field-oriented control (FOC)--based backstepping controller designed for the IPMSM. The EKF observer is utilized for speed and position estimation of the IPMSM, which is discussed in Section 4. Simulation examples are presented in Section 5 to illustrate the effectiveness of the proposed method. Finally, Section 6 provides concluding remarks.

2. The mathematical model of IPMSM

In this section, the dynamic model required for the analysis and control of the IPMSM is built. The structure and equivalent circuit of a two-pole, three-phase star-connected PMSM are shown in Fig.1.

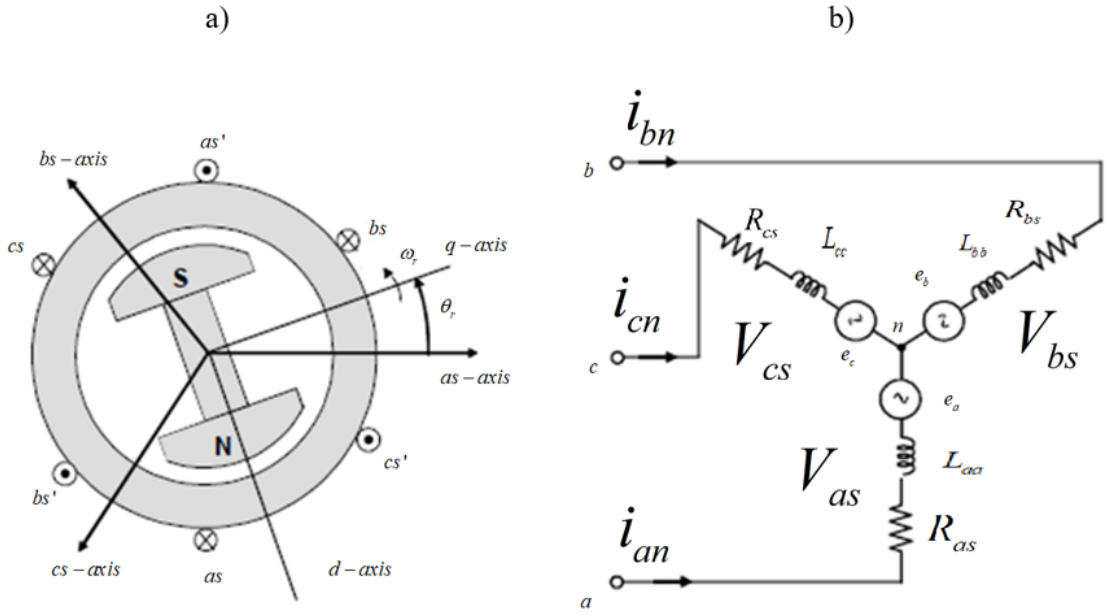

Figure 1. a) structure and b) equivalent circuit of IPMSM.

According to Fig.1, the stator voltage equations of the machine can be written as in Eq.1

$$\boldsymbol{v}_{abcs} = \boldsymbol{R}_s \boldsymbol{i}_{abcs} + \frac{d\boldsymbol{\psi}_{abcs}}{dt}$$

$$\boldsymbol{R}_s = diag[R_s \quad R_s \quad R_s]$$

$$\boldsymbol{\psi}_{abcs} = \boldsymbol{L}_s \boldsymbol{i}_{abcs} + \boldsymbol{\psi}_m$$

$$\boldsymbol{\psi}_m = \psi_m \begin{bmatrix} \sin(\theta_e) \\ \sin\left(\theta_e - \frac{2\pi}{3}\right) \\ \sin\left(\theta_e - \frac{4\pi}{3}\right) \end{bmatrix} \tag{1}$$

where $\boldsymbol{v}_{abcs}$ stator voltages, $\boldsymbol{i}_{abcs}$ stator currents, $\boldsymbol{R}_s$ stator winding resistance matrix, $\boldsymbol{L}_s$ stator inductance matrix, $\boldsymbol{\psi}_{abcs}$ stator fluxes, $\boldsymbol{\psi}_m$ rotor flux provided by permanent magnets, θ_e rotor electrical position, respectively.

Since the inductance matrix $\boldsymbol{L}_s$ given in the model is a function of the rotor's electrical position θ_e and must be differentiated within the model, the current model of IPMSM is quite complex. Various axes transformations can be made to free the inductance matrix from dependence on the rotor position, facilitate the analysis of the machine model, and simplify the control algorithms. Clarke transform is utilized to reduce three-phase quantities in the fixed plane to two phases perpendicular to each other. These two phases are called α and β. Likewise, two-phase quantities that are also in the fixed plane and differ by 90° between them can be converted to three-phase quantities in the fixed plane. This time the transformation is called the inverse Clarke transform. The Clarke transform takes place in the fixed plane. However, as will be mentioned frequently in control, it is also necessary to switch from a fixed plane to a rotating plane or from a rotating plane to a fixed plane. This transformation is possible by using the Park transformation. In this plane, the phases are called d and q. The inverse of the Park transformation is also possible, which means a transition from a two-phase moving plane rotating with speed θ to a two-phase fixed plane. Modeling the PMSM in the $d-q$ axis set in Fig.1a provides great convenience in the control algorithm. Since these axes are fixed to the rotor axis, it is also called rotor-referenced axes. The d axis is in the direction of rotor flux and the q axis is 90^o perpendicular to the d axis. In electrical machine models, voltage, current, and flux transformation matrices, which are vector quantities in axis set transformations, are transformed as in Eq.2.

$$\boldsymbol{f}_{qd0s} = \boldsymbol{K}_s \boldsymbol{f}_{abcs} \tag{2}$$

where $\boldsymbol{K}_s$ is the transformation matrix, $\boldsymbol{f}_{abcs}$ is equal to $[f_{as} \quad f_{bs} \quad f_{cs}]^T$

To switch from the stator $a-b-c$ axis set to the rotor dq axis set, first, the Clarke transformation and then the Park transform are applied. Accordingly, $\boldsymbol{K}_s$ matrix to be used for the transformation will be as follows in Eq.3

$$\boldsymbol{K}_s = \frac{2}{3}\begin{bmatrix} \cos(\theta_e) & \cos\left(\theta_e - \frac{2\pi}{3}\right) & \cos\left(\theta_e - \frac{4\pi}{3}\right) \\ \sin(\theta_e) & \sin\left(\theta_e - \frac{2\pi}{3}\right) & \sin\left(\theta_e - \frac{4\pi}{3}\right) \\ \frac{1}{2} & \frac{1}{2} & \frac{1}{2} \end{bmatrix} \tag{3}$$

Accordingly, if $\boldsymbol{v}_{abcs}$, $\boldsymbol{i}_{abcs}$, and $\boldsymbol{\psi}_{abcs}$ are converted to the quantities in the $d-q$ axis according to Eq.2 with the transformation matrix given in Eq.3, the flux and voltage equations regarding the mathematical model of the IPMSM in the rotor reference system ($d-q$ axis) are written as follows in Eq.4.

$$V_{ds} = R_s i_{ds} + \frac{d\psi_{ds}}{dt} - \omega_e \psi_{qs}$$

$$V_{qs} = R_s i_{qs} + \frac{d\psi_{qs}}{dt} + \omega_e \psi_{ds}$$

$$\psi_{ds} = L_d i_{ds} + \psi_m$$

$$\psi_{qs} = L_q i_{qs}$$

$$\frac{di_{ds}}{dt} = -\frac{R_s}{L_d} i_{ds} + \frac{L_q}{L_d} \omega_e i_{qs} + \frac{1}{L_d} v_{ds}$$

$$\frac{di_{qs}}{dt} = -\frac{R_s}{L_q} i_{qs} - \frac{L_d}{L_q} \omega_e i_{ds} - \frac{1}{L_q} \omega_e \psi_m + \frac{1}{L_q} v_{qs}$$

$$T_e = \frac{3}{2} p\left[\psi_m i_{qs} + \left(L_d - L_q\right) i_{ds} i_{qs}\right]$$

$$\omega_e = \mathrm{p}\omega_\mathrm{m}$$

$$\frac{\mathrm{d}\omega_\mathrm{m}}{\mathrm{dt}} = \frac{1}{J}\mathrm{T_e} - \frac{1}{J}\mathrm{T_L} - \frac{\mathrm{B}}{J}\omega_\mathrm{m}$$

$$\frac{d\theta_e}{dt} = \omega_e = p\omega_m$$

$$P = \frac{3}{2}\mathrm{R_s}\left(\mathrm{i_{ds}^2} + \frac{4\mathrm{T_e^2}}{9p^2\left[\psi_m + \left(\mathrm{L_d} - \mathrm{L_q}\right)\mathrm{i}_{ds}\right]^2}\right) \tag{4}$$

where p is the number of pole pairs; R_s is the stator winding resistance; ω_e is the electrical angular frequency; ω_m is the mechanical angular frequency; $V_{ds}, V_{qs}, i_{ds}, i_{qs}$ are stator winding voltage and currents projected into the $d-q$ axis, respectively; ψ_{ds}, ψ_{qs} are stator flux projected into the $d-q$ axis; ψ_m is the rotor flux linkage, L_d and L_q are the stator inductances reflected into the $d-q$ axis; T_e is the motor's electrical torque; T_L is the load torque; J is the rotor inertia; B is the viscous friction coefficient; P is the electrical power.

To formulate the design problem, according to Eq.4, the state-space model of the IPMSM is constructed as the following nonlinear system in Eq.5

$$\overbrace{\begin{bmatrix}\dot{x}_1\\ \dot{x}_2\\ \dot{x}_3\end{bmatrix}}^{\dot{x}(t)}=\begin{bmatrix}-\frac{B}{J} & \frac{3p\psi_m}{2J} & 0\\ -\frac{p\psi_m}{L_q} & -\frac{R_s}{L_q} & -px_1\\ 0 & px_1 & -\frac{R_s}{L_d}\end{bmatrix}\overbrace{\begin{bmatrix}x_1\\ x_2\\ x_3\end{bmatrix}}^{x(t)}+\begin{bmatrix}-\frac{T_L}{J}\\ \frac{V_{qs}}{L_q}\\ \frac{V_{ds}}{L_d}\end{bmatrix} \tag{5}$$

where $x(t)$ is the state vector. x_1, x_2, x_3 correspond to the $\omega_m\,(rotor\ speed)$, $i_{qs}\ (stator\ quadrature\ current), i_{ds}(stator\ direct\ current)$, respectively.

The main control objective is confining all closed-loop signals bounded and satisfying global asymptotic convergence of the speed and current tracking errors to zero.

3. Controller Design

3.1.Backstepping Controller Design

Backstepping control is an efficient nonlinear control system method, whose first step is to define a virtual control state. Then, the state is forced to be a stabilizing function. The control input is designed considering Lyapunov stability so that the error variable is stabilized [65-67].

3.1.1.Speed controller

The controller for the speed state x_1 is designed to achieve speed tracking problems, therefore the state tracking error variable is defined as in Eq.6

$$e_1 = x_1^* - x_1 \tag{6}$$

where x_1^* is the reference rotor speed.

To stabilize the speed component, the speed tracking error dynamics are derived using Eq.5 and Eq.6 as in Eq.7

$$\dot{e}_1 = \dot{x}_1^* - \dot{x}_1 = \frac{T_L}{J} + \frac{B}{J}x_1 - \frac{3p\psi_m}{2J}x_2 \tag{7}$$

The following Lyapunov function candidate is chosen as in Eq.8

$$V_1 = \frac{1}{2}e_1^2 \tag{8}$$

The time derivative of the Lyapunov function is expressed as in Eq.9

$$\dot{V}_1 = e_1\dot{e}_1 = \frac{e_1}{J}\left(Bx_1 + T_L - \frac{3p\psi_m}{2}x_2 \right) \tag{9}$$

By utilizing Lypunov's stability definition ($\dot{V}_1 \prec 0$), to make the tracking error convergence to zero, Eq.10 must be satisfied

$$\frac{e_1}{J}\left(Bx_1 + T_L - \frac{3p\psi_m}{2}x_2 \right) = -k_0 e_1^2, k_0 \succ 0 \tag{10}$$

The backstepping methodology dictates that the virtual control variable input x_2 is found by solving Eq.10 for x_2 as in Eq.11.

$$x_2^* = \frac{2}{3p\psi_m}\left(Bx_1 + T_L + k_0 J e_1 \right) \tag{11}$$

If Eq.11 is satisfied, the speed error approaches zero, i.e., global asymptotic tracking of speed is guaranteed.

Decoupling nonlinear control is utilized in the IPMSM control system. The exact thrust force that drives the motor is obtained by the stator quadrature current (x_2). When the stator direct current (x_3) is forced to drive zero, the coupling term x_1, x_3 in Eq.4 is eliminated and power consumption is minimized in terms of control action.

When $i_{ds} = x_3 = 0$, the control scheme should be $x_3^* = 0$.

3.1.2.Current controller

To satisfy the q-axis current tracking e_2 is chosen as a new state variable given in Eq.12

$$e_2 = x_2^* - x_2 \tag{12}$$

The derivative of the e_2 is evaluated as in Eq.13

$$\dot{e}_2 = \dot{x}_2^* - \dot{x}_2 = \frac{2}{3p\psi_m}\left(B\dot{x}_1 + \dot{T}_L + k_0 J\dot{e}_1 \right) + \frac{R_s}{L_q}x_2 + px_1x_3 + \frac{p\psi_m}{L_q}x_1 - \frac{v_{qs}}{L_q}$$
$$= \frac{Bx_2}{J} - k_0x_2 - \frac{v_{qs}}{L_q} + \frac{R_sx_2}{L_s} + px_1x_3 + \frac{2\dot{T}_Lk_0}{3p\psi_m} + \frac{2T_Lk_0}{3p\psi_m} + \frac{p\psi_mx_1}{L_s} - \frac{2B^2x_1}{3Jp\psi_m} - \frac{2BT_L}{3Jp\psi_m} + \frac{2Bk_0x_1}{3p\psi_m} \tag{13}$$

For the new system based on e_1 and e_2, the second Lyapunov function is defined as in Eq.14

$$V_2 = V_1 + \frac{1}{2}e_2^2 \tag{14}$$

The time derivative of V_2 is given as in Eq.15

$$\dot{V}_2 = e_1\dot{e}_1 + e_2\dot{e}_2 = e_1\left(\frac{T_L}{J} + \frac{B}{J}x_1 - \frac{3p\psi_m}{2J}x_2\right)$$
$$+e_2\left(\frac{Bx_2}{J} - k_0x_2 - \frac{v_{qs}}{L_q} + \frac{R_sx_2}{L_s} + px_1x_3 + \frac{2\dot{T}_Lk_0}{3p\psi_m} + \frac{2T_Lk_0}{3p\psi_m} + \frac{p\psi_mx_1}{L_s} - \frac{2B^2x_1}{3Jp\psi_m} - \frac{2BT_L}{3Jp\psi_m} + \frac{2Bk_0x_1}{3p\psi_m}\right) \tag{15}$$

By utilizing Lypunov's stability definition ($\dot{V}_2 \prec 0$), to make the tracking error convergence to zero, Eq.16 must be satisfied

$$\dot{V}_2 = -k_0e_1^2 - k_1e_2^2, k_1 \succ 0 \tag{16}$$

The stabilizing control law is derived from Eq.16 ($\dot{e}_2 = -k_1e_2$) by solving the actual control variable v_{qs} as in Eq.17

$$v_{qs}^* = R_sx_2 - L_sk_0x_2 + p\psi_mx_1 + L_sk_1e_2 + \frac{BL_sx_2}{J} + \frac{2L_s\dot{T}_L}{3p\psi_m} + L_spx_1x_3 + \frac{2L_sk_0T_L}{3p\psi_m} - \frac{2B^2L_sx_1}{3Jp\psi_m} + \frac{2BL_sk_0x_1}{3p\psi_m} - \frac{2BL_sT_L}{3Jp\psi_m} \tag{17}$$

Similarly, the d-axis current controller can be designed by choosing d-axis current tracking error as a new state variable as in Eq.18

$$e_3 = x_3^* - x_3 \tag{18}$$

Differentiating e_3 concerning time and using the results of Eq.4, Eq.19 is obtained

$$\dot{e}_3 = \frac{R_sx_3}{L_s} - \frac{v_{ds}}{L_s} - px_1x_2 \tag{19}$$

For a new system based on three errors, the third Lyapunov function is stated as in Eq.20

$$V_3 = V_2 + \frac{1}{2}e_3^2 \tag{20}$$

Differentiating V_3 for time, Eq.21 is obtained

$$\dot{V}_3 = \dot{V}_2 + e_3\dot{e}_3 = \dot{V}_2 + e_3\left(\frac{R_s x_3}{L_s} - \frac{v_{ds}}{L_s} - px_1x_2\right) \tag{21}$$

Eq.21 contains the actual control variable v_{ds}. By utilizing Lypunov's stability definition ($\dot{V}_3 \prec 0$), To make the tracking error converge to zero, Eq.22 must be satisfied

$$\dot{V}_3 = -k_0e_1^2 - k_1e_2^2 - k_2e_3^2, k_2 \succ 0 \tag{22}$$

The stabilizing control law is derived from Eq.22 ($\dot{e}_3 = -k_2e_3$) by solving the actual control variable v_{ds} as in Eq.23

$$v_{ds}^* = R_s x_3 + L_s k_2 e_3 - L_s p x_1 x_2 \tag{23}$$

The objective of backstepping control for IPMSM is completed.

3.2.Field-Oriented Vector Control

FOC allows for the separation of the magnetizing flux and torque flux components of the stator currents, so it is possible to control the torque independent of magnetization. According to the electromagnetic laws, the torque created in the synchronous machine is equal to the vector product of the magnetic fields existing in the machine as given in Eq.24

$$\boldsymbol{T}_e = \boldsymbol{B}_{stator} \times \boldsymbol{B}_{rotor} \tag{24}$$

A PMSM consists of a permanent magnet rotating in the rotor and symmetrical windings placed in the stator surrounding it. The field vector created by the current flowing through each winding is combined with the field vectors created by the other windings to form the total magnetic field vector ($\boldsymbol{B}_{stator}$). It is possible to create a magnetic field of any direction and amplitude in the air gap by controlling the current flowing in each winding. The torque is produced by the attraction or repulsion between the total stator magnetic field strength and the rotor magnetic field strength. According to Eq.24, in any rotor position, there is a net stator field direction that makes the torque the highest, as well as a direction that makes the torque zero. If a net stator field is produced in the same direction as the field produced by the permanent magnet rotor, no torque is produced. The fields affect each other to produce a force, but since the force is in line with the direction of rotation of the rotor, it does not rotate the motor, it just compresses the bearings. On the other hand, if the stator field is perpendicular to the field

produced by the rotor, magnetic forces try to rotate the rotor, and the torque is maximized. A stator field chosen in any direction and size can be divided into perpendicular and parallel components of the rotor field. In this case, the perpendicular component produces torque, while the parallel component generates a useless compression force. Therefore, an efficient PMSM driver will increase the perpendicular component of the stator field while decreasing the component parallel to the rotor field. While designing and modeling the control system, current windings are used as control variables instead of stator magnetic field, since magnetic field intensities cannot be measured directly. In PMSM, the stator field vector is produced by three-phase windings placed at a geometric angle of 120°. There is a 120° phase difference between the field vectors produced by each winding. The net magnetic stator field is produced by the sum of these three components. "Current space vectors" are used to model the fields produced by the stator windings in terms of winding currents. The current space vector of a winding is in the direction of the field vector produced by the winding and its amplitude is proportional to the current flowing through the winding. This allows the total stator field to be represented by a current space vector that is the sum of the current space vector of the three phases. The current space vector is an apparent current flowing through a rotating apparent (imaginary) winding, introduced to relate the direction and amplitude of the real stator field to the current flowing through the stator windings. As in the stator field, the stator current space vector can be divided into components perpendicular and parallel to the axis of the rotor magnet. The longitudinal axis current component generates a magnetic field at appropriate angles to the rotor magnet, which generates torque. The transverse axis current component produces a field parallel to the rotor magnet, which does not produce torque. Because bearing wear causes problems such as heating, transverse axis currents are always set to zero in a good control algorithm. In this case, the moment will be proportional to the amplitude of the current space vector. To efficiently produce a constant uniform torque, the stator current space vector must be of constant magnitude and rotate with the rotor to lie on the longitudinal axis, regardless of rotor position and speed. Although the stator current space vector is of constant magnitude and direction when viewed from the rotating rotor axis, it draws a circle as the motor rotates when viewed from the fixed stator axis. The current space vector is produced by the sum of the vector components of each of the motor windings and each of the three windings is located at a geometric angle of 120°. Motor currents should preferably be sinusoidal and have a phase difference of 120° between them. Sinusoidal winding currents depend on the rotor angle, so the transverse axis component of the stator current space vector is zeroed while the longitudinal axis component is made as high as possible. Vector control is a method that enables these machines to be

controlled like a direct current motor by reducing the stator currents of a three-phase alternating current motor to two components perpendicular to each other in variable-speed drive systems. One component creates the flux of the motor, while the other component creates the torque. The current components that make up the reference torque and flux are compared with the currents of the motor reduced to two components. A controller keeps the measured current components constant in the reference current component. According to the output of the PI controller, the semiconductor power elements in the inverter (variable speed drive systems) are switched. Vector control induction motor is used quite often in PMSMs. Thanks to vector control, it is possible to control in a wide speed range. In addition, rated torque at zero speed can be achieved and the dynamic performance of the system can be significantly improved. In FOC, the current and voltages of the motor are controlled at the $d-q$ reference axes of the rotor. It is the mathematical conversion of the measured motor current from the three-phase fixed axis set of the stator windings to the two-axis rotational $d-q$ reference axes before it enters the controller. Similarly, before the voltage applied to the motor is used at the output of the pulse width modulator (PWM), it must be mathematically converted from the $d-q$ reference axes of the rotor to the three-phase reference axes of the stator. These transformations, which are the basis of FOC, usually require DSPs or high-performance processors with fast mathematical processing capability. Indirect field-directed control or vector control has become the standard for AC drives with speed and torque control to achieve high dynamic motor behavior. Torque control of PMSM in constant torque region is done by rotor reference plane quadrature axis (i_{qs}) current. This region is the region up to the motor-rated speed. The constant power region is the region for speeds after the rated speed of the motor. In this region, besides the quadrature axis current of the motor (i_{qs}), the direct axis current (i_{ds}) is also controlled. In vector control methods, the use of phase transformations provides simplicity in motor dynamic equations.

Indirect vector control is summarized below:

Step 1: Two of the three stator phase currents are measured and the third current is determined using Kirchoff's current law ($i_{as}+i_{bs}+i_{cs}=0$).

Step 2: Three-phase currents are converted from a 3-axis stator system to a 2-axis stator-based coordinate system using Clarke transformation $\left(i_{as},i_{bs},i_{cs}\right)\Rightarrow\left(i_{\alpha s},i_{\beta s}\right)$.

Step 3: The components in the two axes of the stator current are time-dependent and very complex to control with a specific controller. Therefore, it is necessary to reduce it to the

reference axis fixed to the rotor. This conversion is done using Park transformation. Instantaneous values of the rotor angle are needed $\left(i_{\alpha s}, i_{\beta s}\right) \Rightarrow \left(i_{ds}, i_{qs}\right)$.

Step 4: The error signals to enter the controller are obtained from the difference between the i_{ds} and i_{qs} currents, the reference currents. The rotor magnetizing flux is controlled concerning i_{ds} and the motor output torque is controlled by reference to i_{qs}. The output of the controller will be the voltage vector v_{ds} and v_{qs} to be sent to the motor**.**

Step 5: Since the rotor angle is required for the FOC algorithm, the v_{ds} and v_{qs} output values from the controller are returned to the stationary reference system using the rotor angle, and the $v_{\alpha s}$ and $v_{\beta s}$ values are calculated. When $i_{\alpha s}$ and $i_{\beta s}$ are inputs, the new conversion angle is estimated. Outputs of controllers are converted back to three-phase stator reference by going through reverse Park and reverse Clarke transformations.

Step 6: The voltages $v_{\alpha s}$ and $v_{\beta s}$ are converted to three-phase voltage v_{as}, v_{bs}, and v_{cs} to obtain pulse width modulated signals that will yield the three-phase voltage at the inverter output. The v_{ds} and v_{qs} output values from the controller are returned to the fixed reference system using the new angle value. The PWM space is tuned using vector shifting by generating a three-phase reference signal.

Since the rotor magnetic field always extends along the d-axis of the rotor $d-q$ axis set, the component of the stator field in the d-axis must be zero and the component of the stator field in the q-axis must be maximum. To efficiently produce a constant uniform torque, the stator field (hence the stator current space vector) must be of constant magnitude on the q-axis, and to achieve this, it must rotate with the rotor regardless of rotor position and speed. The flux and torque control algorithm tries to keep the resultant stator magnetic field always on the q −axis of the rotor by adjusting the stator winding voltages and making its d −axis component zero. FOC allows controlling separately the component of the stator magnetic field formed by the stator currents on the q-axis and the torque, and the magnetization with the component on the d-axis. There are two separate current control loops for the q and d components of the stator currents. The block diagram of the speed control of FOC is given in Fig.2.

Since the motor torque is directly dependent on the quadrature current i_{qs}, controlling the i_{qs} means controlling the torque. The output of the speed controller is the reference current i_{qs}. The reference of the i_{ds} current should be zero throughout the operation. The output of the i_{qs} and i_{ds} current controllers are the voltages v_{qs} and v_{ds}, which must be applied to the motor, respectively.

As can be seen, in FOC, the current and voltages of the motor are controlled at the $d-q$ reference frame of the rotor. The mathematical conversion of the measured motor current from the three-phase $a-b-c$ axis set of the stator windings, first to the fixed α-β axis set of the stator (Clarke transform), and then to the rotor $d-q$ reference axis set (Park transform), before entering the controller. Similarly, the voltage to be applied to the motor is mathematically converted from the $d-q$ reference axis set of the rotor to α-β (Inverse Park transform) components on the fixed stator axis set before it is used in the PWM. The purpose of the transformation in all these reference axes is to save the time-varying sinusoidal motor current and voltage signals from the dependence of time and to transform them into a direct current signal. In FOC, since the reference currents are constant in the $d-q$ reference frame, the controller operates in DC mode instead of a sinusoidal signal. This isolates the controller from time-dependent current and voltage, thus eliminating the frequency response limitation of the controller and the phase shift on the torque and speed of the motor. The quality of current control becomes independent of the angular speed of the motor and it is possible to control over a wide speed range. In addition, maximum torque control at zero speed can be achieved and the dynamic performance of the system can be significantly improved.

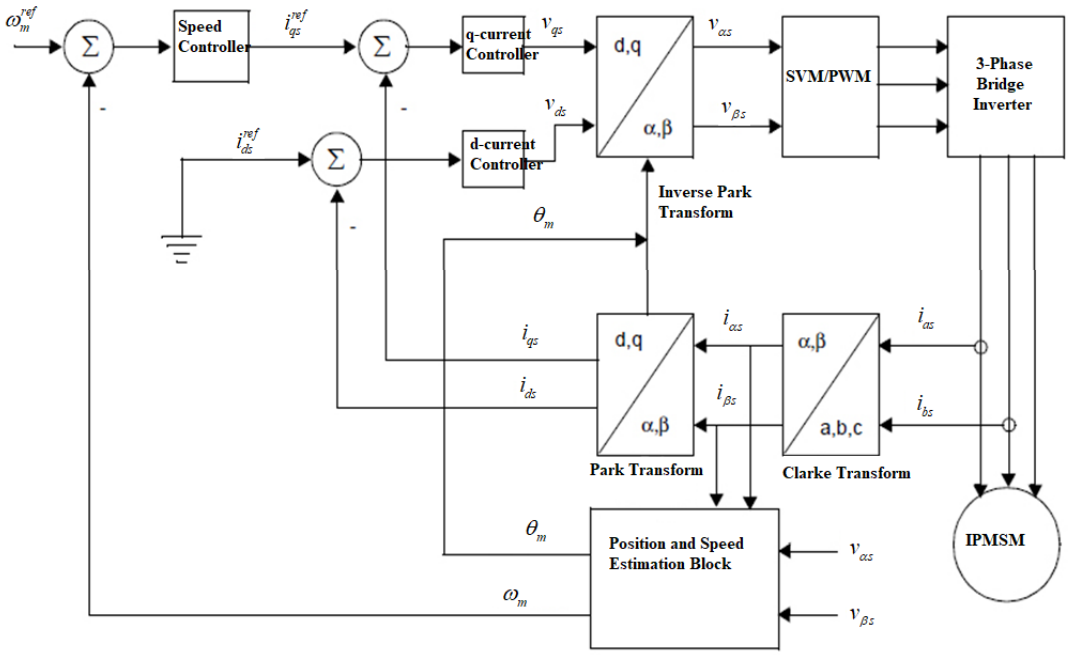

Figure 2. Field-oriented control block diagram of PMSM.

4. Extended Kalman Filter (EKF)

Extended Kalman filter (EKF), which is a stochastic method due to its success in state estimation in non-linear systems, is widely used for estimating rotor position and speed in synchronous motor drives. EKF is an optimal estimator using the least squares method for state estimation in dynamic nonlinear systems [68, 69].

In a non-linear discrete-time system; system noises (w_k) including system disturbances and model uncertainties and the measurement noises (v_k) are represented in Eq.25 with zero-mean white Gaussian noise having covariance matrices Q_k and R_k , respectively,

$$\begin{aligned} x_k &= f\left(x_{k-1}\right) + w_{k-1} \\ z_k &= h\left(x_k\right) + v_k \end{aligned} \tag{25}$$

Here, $f\left(x_{k-1}\right)$ shows the nonlinear state equations of the system. The initial value of states (x_0) is a random vector with covariance $P_0 = E\left[\left(x_0 - \mu_0\right)\left(x_0 - \mu_0\right)^T\right]$ and mean value $\mu_0 = E\left[x_0\right]$. The w_k v_k noises are uncorrelated to each other and the initial state vector x_0.

The following relations given in Eq.26 are valid [70, 71].

$$
\begin{aligned}
&E\left[w_k\right]=E\left[v_k\right]=0\\
&E\left[w_k {w_k}^T\right]=Q_k\\
&E\left[v_k {v_k}^T\right]=R_k\\
&E\left[w_k {w_j}^T\right]=0,\ k\neq j\\
&E\left[v_k {v_j}^T\right]=0,\ k\neq j\\
&E\left[w_k {x_0}^T\right]=0,\ \forall k\\
&E\left[v_k {x_0}^T\right]=0,\ \forall k\\
&E\left[w_k {v_j}^T\right]=0,\ \forall k\ ve\ \forall j
\end{aligned}
\tag{26}
$$

The algorithm consists of two steps. ***Step 1:*** Predict the next state using the previous state estimation; ***Step 2:*** Update/correct the previous estimate by looking at the measured values.

The pseudocode scheme of the EKF algorithm is given in Table 1 [72, 73].

Table 1: The pseudocode scheme of the EKF algorithm.

Initialization Step:

$x_0(\mu_0, P_0)$, an initial error covariance matrix

Estimation Step:

$$
\begin{aligned}
&\overline{x}_k = f\left(\hat{x}_{k-1}\right) \quad or \quad \overline{x}_k = \hat{x}_{k-1} + f\left(\hat{x}_{k-1}\right)T_s\\
&\overline{P}_k = J_f\left(\hat{x}_{k-1}\right)P_{k-1}{J_f}^T\left(\hat{x}_{k-1}\right)+Q_{k-1}\\
&or\\
&\overline{P}_k = P_{k-1}+\left[J_f\left(\hat{x}_{k-1}\right)P_{k-1}+P_{k-1}{J_f}^T\left(\hat{x}_{k-1}\right)\right]T_s+Q_{k-1}
\end{aligned}
$$

Update Step:

$$
\begin{aligned}
&\hat{x}_k = \overline{x}_k + K_k\left(z_k - h\left(\overline{x}_k\right)\right)\\
&K_k = \overline{P}_k {J_h}^T\left(\overline{x}_k\right)\left[J_h\left(\overline{x}_k\right)\overline{P}_k {J_h}^T\left(\overline{x}_k\right)+R_k\right]^{-1}\\
&P_k = \left[I - K_k J_h\left(\overline{x}_k\right)\right]\overline{P}_k
\end{aligned}
$$

where values written with "^" represent optimal estimations. The optimal gain that makes the best prediction is known as the Kalman gain (K_k). $J_f\left(.\right)$, $J_h\left(.\right)$ are the linear Jacobian matrices of nonlinear equations of state matrices ($f\left(.\right), h\left(.\right)$), respectively. If the state equations

are linear, the Jacobian matrices are written as follows in Eq.27

$$\begin{aligned} x_k &= \underbrace{A\,x_{k-1} + B\,u_{k-1}}_{f(x_{k-1})} + w_{k-1} \quad \rightarrow \quad J_f\left(\hat{x}_{k-1}\right) = A \\ z_k &= \underbrace{C\,x_k}_{h(x_k)} + v_k \qquad\qquad\quad \rightarrow \quad J_h\left(\bar{x}_k\right) = C \end{aligned} \tag{27}$$

4.1. Application of EKF Algorithm to IPMSM

The dynamic equations of IPMSM in the $\alpha - \beta$ axis set are as in Eq.28 [74].

$$\begin{aligned} \frac{di_{\alpha s}}{dt} &= -\frac{R_s}{L_s} i_{\alpha s} + \frac{\omega_m \psi_m}{L_s} \sin\theta_m + \frac{V_{\alpha s}}{L_s} \\ \frac{di_{\beta s}}{dt} &= -\frac{R_s}{L_s} i_{\alpha s} - \frac{\omega_m \psi_m}{L_s} \cos\theta_m + \frac{V_{\beta s}}{L_s} \\ \frac{d\theta_m}{dt} &= \omega_m \end{aligned} \tag{28}$$

If the state variables of the machine state space model are selected as $x = \begin{bmatrix} i_{\alpha s} & i_{\beta s} & \omega_m & \theta_m \end{bmatrix}^T$ the EKF equations are stated in Eq.29.

$$f\left(x(t)\right) = \begin{bmatrix} f_1 \\ f_2 \\ f_3 \\ f_4 \end{bmatrix} = \begin{bmatrix} -\frac{R_s}{L_s} i_{\alpha s} + \frac{\omega_m \psi_m}{L_s} \sin\theta_m + \frac{V_{\alpha s}}{L_s} \\ -\frac{R_s}{L_s} i_{\alpha s} - \frac{\omega_m \psi_m}{L_s} \cos\theta_m + \frac{V_{\beta s}}{L_s} \\ 0 \\ \omega_m \end{bmatrix}$$

$$z = \begin{bmatrix} i_{\alpha s} & i_{\beta s} \end{bmatrix}^T$$

$$\begin{aligned} x_k &= f\left(x_{k-1}\right) + w_{k-1} \\ z_k &= C\,x_k + v_k \end{aligned}$$

$$J_f = \left.\frac{\partial f}{\partial x}\right|_{x=x(t)} = \begin{bmatrix} -\frac{R_s}{L_s} & 0 & \frac{\psi_m}{L_s}\sin\theta_m & \frac{\omega_m \psi_m}{L_s}\cos\theta_m \\ 0 & -\frac{R_s}{L_s} & -\frac{\psi_m}{L_s}\sin\theta_m & \frac{\omega_m \psi_m}{L_s}\sin\theta_m \\ 0 & 0 & 0 & 0 \\ 0 & 0 & 1 & 0 \end{bmatrix} \tag{29}$$

An important point in EKF design is the determination of covariance matrices, which is often done by trial and error. A sensorless backstepping control block diagram of EKF-based IPMSM is demonstrated in Fig.3.

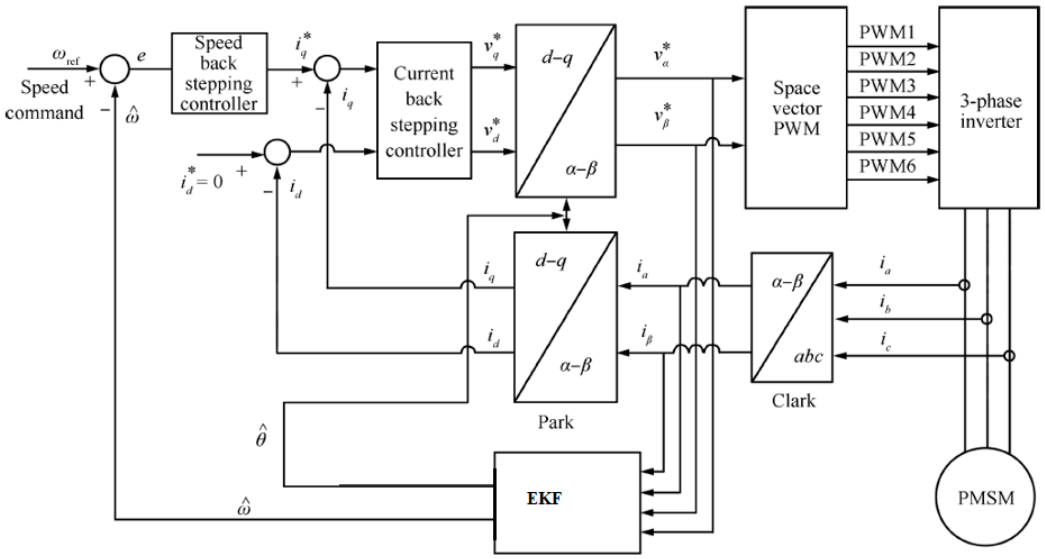

Figure 3. Sensorless backstepping control block diagram of EKF-based IPMSM.

5. Simulation Results

The simulations were conducted using the Matlab/Simulink program. EKF was implemented to estimate internal states in the model. The observer was designed with the requirements to have a higher bandwidth than the overall control loop. The EKF code was created via an s-function block and then put into the Simulink model. The parameters and the rated sizes of the motor used in the simulation are given in Table 2.

Table 2. Motor sizes and parameters used in the simulation.

Parameter	Value
Rated power	9 kW
Rated torque	20 Nm
Rated speed	4000 rev/min
R_s	2.48 Ω
$L_d = L_q$	14 mH
ψ_m	0.105 Vs/rad
p	2
J	0.02 kgm^2
B	0.001 Nms/rad

A critical step in the construction of the EKF is the selection of the elements of the covariance matrices **Q** and **R**, as they will determine the performance, stability, and convergence. The large values of **Q** increase model noise and/or parameter uncertainties. Therefore the filter dynamics are getting faster, while steady-state performance is getting poorer. **R** matrix is associated with the measurement noise. Increasing the values of the elements in **R** leads to poorer transient response. The covariances are fixed for the simulations. The following values were selected:

$$P_0 = \begin{bmatrix} 0.01 & 0 & 0 & 0 & 0 \\ 0 & 0.01 & 0 & 0 & 0 \\ 0 & 0 & 0.01 & 0 & 0 \\ 0 & 0 & 0 & 0.01 & 0 \\ 0 & 0 & 0 & 0 & 10 \end{bmatrix}; Q = \begin{bmatrix} 0.4 & 0 & 0 & 0 & 0 \\ 0 & 0.004 & 0 & 0 & 0 \\ 0 & 0 & 200 & 0 & 0 \\ 0 & 0 & 0 & 2 & 0 \\ 0 & 0 & 0 & 0 & 0.01 \end{bmatrix};$$

$$R = \begin{bmatrix} 0.0374 & 0 \\ 0 & 0.0374 \end{bmatrix}$$

After various simulation experiments having different Q and R matrices, it was concluded that those values give a good transient response and steady-state performance. Fig.4 shows the simulation results of EKF state estimation performance and backstepping controller trajectory tracking performance for the sensorless IPMSM drive.

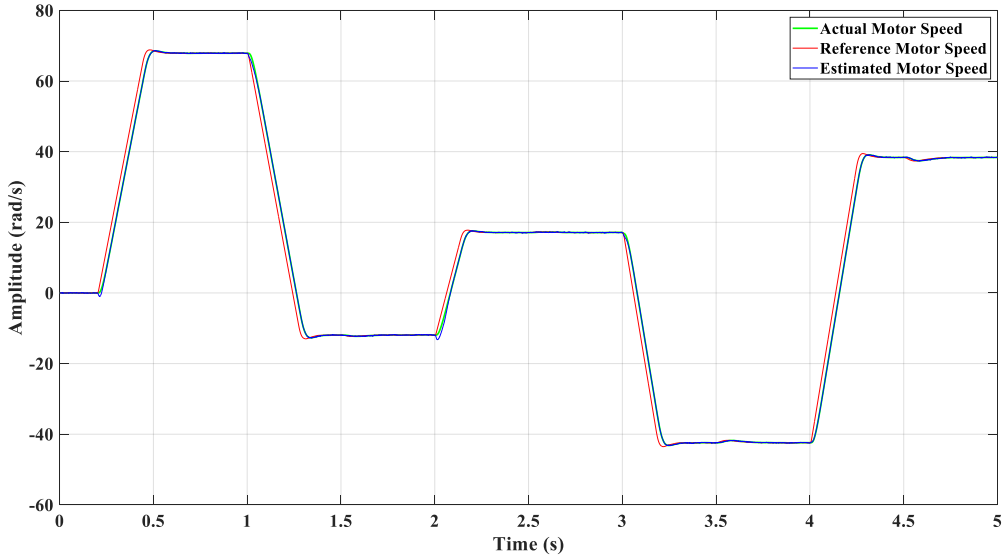

Figure 4: EKF estimation and backstepping controller performance: motor speed state for no-load speed variation and speed reversal.

It can be stated that EKF is capable of tracking the speed state satisfactorily under noisy machine operation. Besides, in Fig.5, the measured and estimated stator currents in the alpha-beta domain are demonstrated.

a)

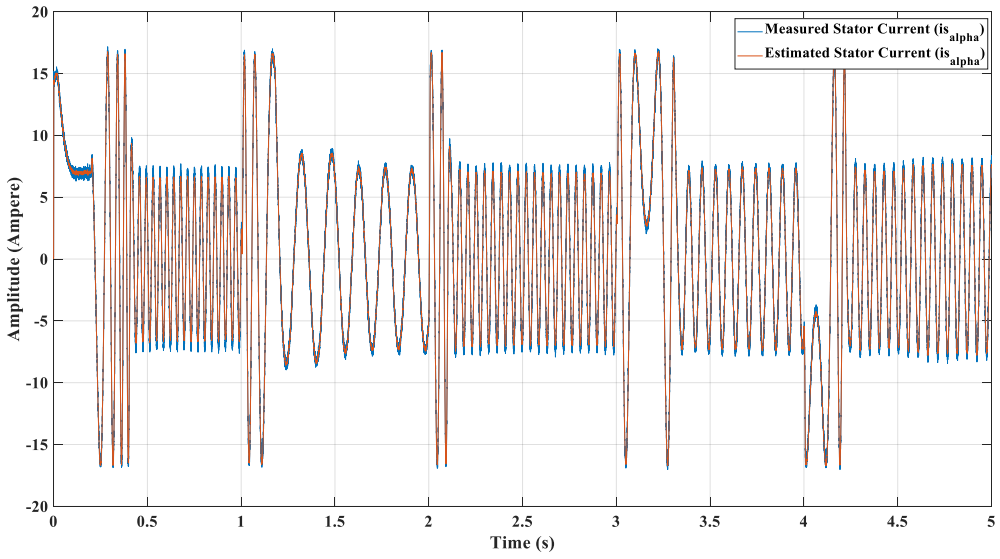

b)

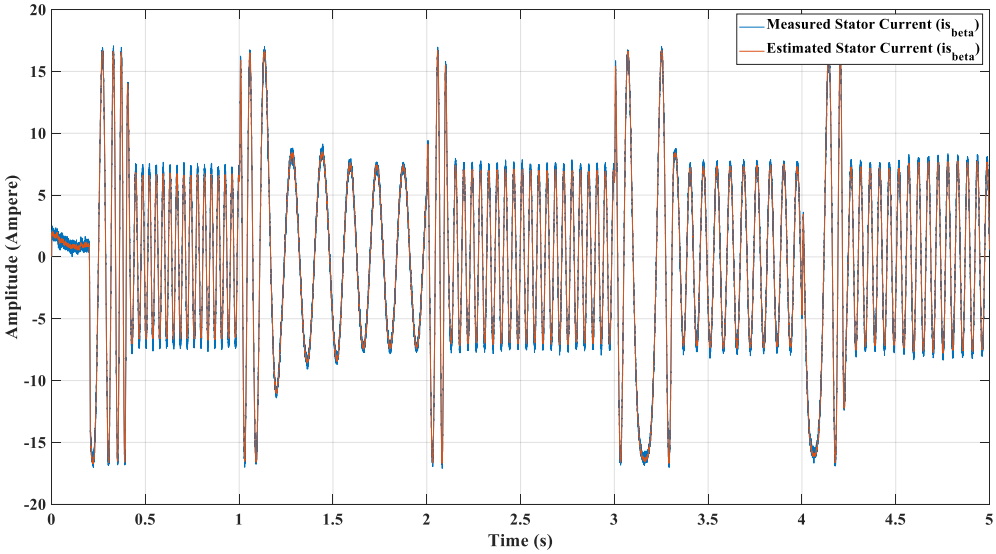

Figure 5: EKF performance: a) measured and estimated stator currents on α-axis, b) measured and estimated stator current on β-axis.

The control is affected by noisy measurements, it can be deduced that the achieved objective of FOC, the EKF gives good estimates of the speed with the rejection of noises, and the control response is improved. In another scenario, the simulation results are given when the reference speed is 400 rad/s and the motor is loaded with a step load of 20 Nm (rated torque) at t=3 s. Fig.6 shows the backstepping control performance under the condition of the load torque variations.

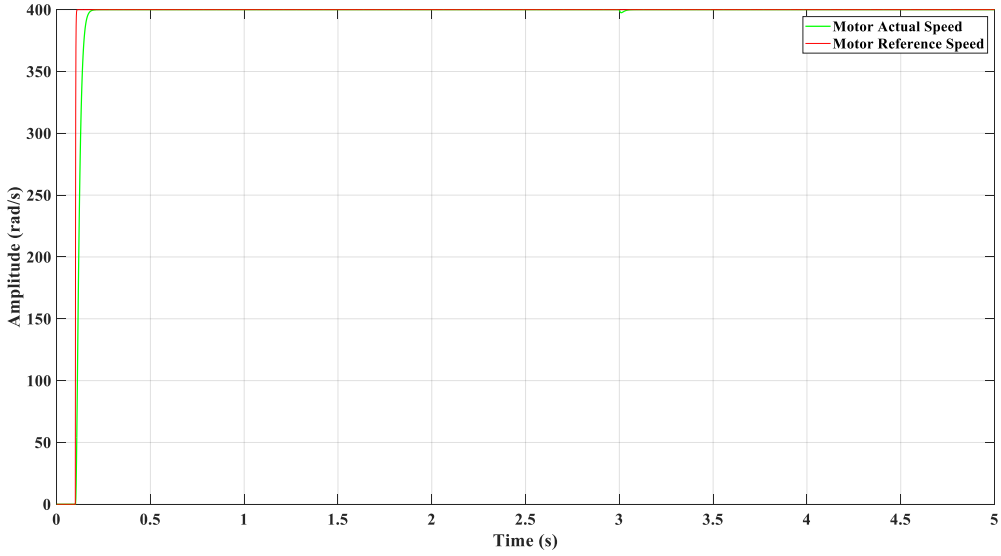

Figure 6: Backstepping control performance: motor speed state under load torque variation.

In Fig.7, the time-dependent variation of stator currents in the direct and quadrature axes is presented.

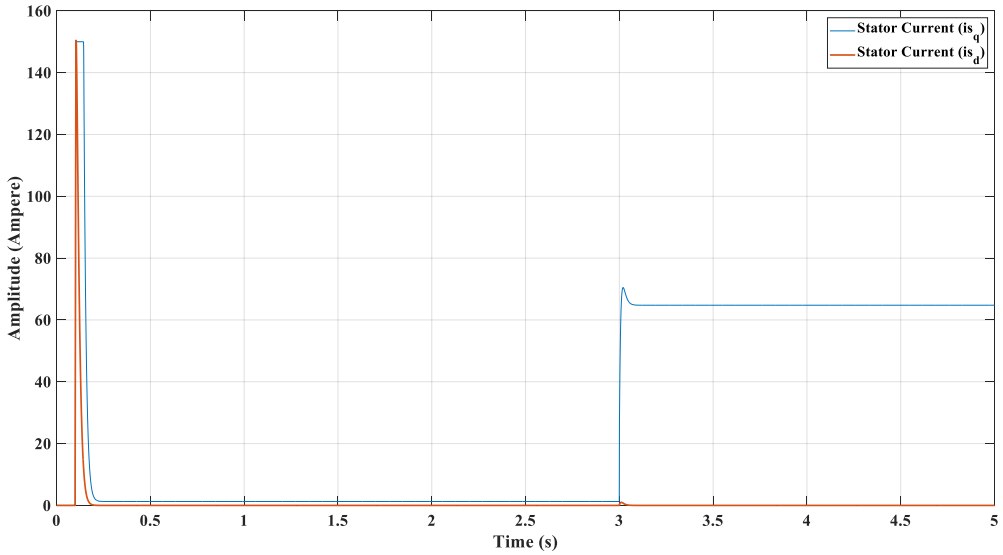

Figure 7: Time-dependent variation of stator currents in direct and quadrature axis.

In Fig.8, the time-dependent variation of motor torque and load torque is demonstrated. The current components of the direct and quadrature axis behave decoupled. The direct axis current is always forced to zero to orient all the linkage flux in the d-axis and achieve maximum torque per ampere.

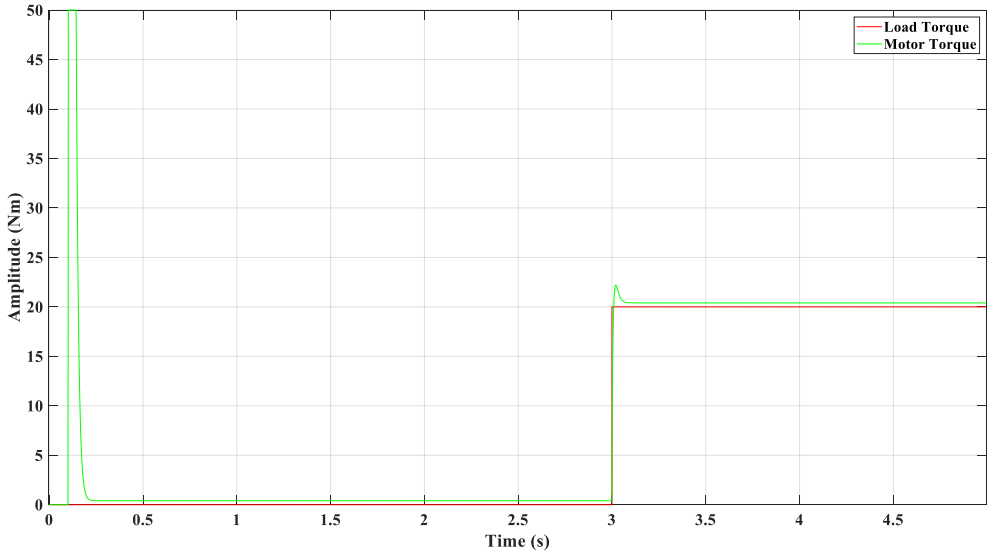

Figure 8: The time-dependent variation of motor torque and load torque.

The results show the effectiveness and fast response without overshoot at tracking a reference speed under parameter and load torque variations throughout the system.

6. Conclusion

The simulation results indicate that EKF is capable of tracking the actual rotor speed and that the elements of the covariance matrices, which are extracted via a trial-and-error process, are properly chosen. The transient response, steady-state performance, and robustness against the noise of the EKF seem satisfactory under the condition of the variable load and speed cases and process uncertainties. EKF is a good choice as the algorithms and models are easier to optimize for real-time implementation, high performance, and low cost for the microprocessors. The simulation results related to the backstepping controller demonstrate excellent speed tracking and anti-disturbance performance while ensuring the asymptotical stability of the system over a large span of operating conditions. The overall methodology gives a significant enhancement in performance and stability. The backstepping technique combined with vector control provides high control performance and robustness Moreover, the elimination of the sensor reduces the constraints and gives more flexibility to control the IPMSM.

Funding Information: The author states no funding is involved.

Author contributions: The author accepted responsibility for the entire content of this manuscript and approved its submission

Conflict of interest: The author states no conflict of interest.

References

1. Vaez-Zadeh S. Control of permanent magnet synchronous motors. Oxford Scholarship Online 2018. Epub ahead of print 2018. DOI: 10.1093/oso/9780198742968.001.0001.

2. Hughes A, Drury B. Electric motors and drives: Fundamentals, types and applications. Kidlington, Oxford, United Kingdom: Elsevier, Newnes, an imprint of Elsevier, 2019.

3. Xia S, Wang S. Design of high-speed high power density single-phase permanent magnet brushless DC motor considering control performance. 2020 IEEE International Conference on Industrial Technology (ICIT) 2020. Epub ahead of print 2020. DOI: 10.1109/icit45562.2020.9067127.

4. Toliyat HA, Kliman GB. Handbook of Electric Motors. New York: Marcel Dekker, 2004.

5. Louis J-P. Control of Synchronous Motors. London: ISTE, 2011.

6. De Soricellis M, Rapp H. Current and voltage shaping method via modified d–q transformation for the torque ripple compensation in PMSMs. The Journal of Engineering; 2019: 3812–3817.

7. Gamazo-Real JC, Vázquez-Sánchez E, Gómez-Gil J. Position and speed control of brushless DC motors using sensorless techniques and application trends. Sensors; 10: 6901–6947.

8. Sain C, Banerjee A, Biswas PK, et al. Sensor angle-based control strategy and dynamic analysis of a sinusoidal pulse width modulation-operated permanent Magnet Synchronous Machine Drive for Electric Propulsion Unit. International Transactions on Electrical Energy Systems 2021; 31. Epub ahead of print 2021. DOI: 10.1002/2050-7038.13090.

9. Laskaris KI, Kladas AG. High torque internal permanent magnet wheel motor for electric traction applications. 2008 18th International Conference on Electrical Machines 2008. Epub ahead of print 2008. DOI: 10.1109/icelmach.2008.4800184.

10. Wu J, Hu Y, Zhang B, et al. Comparison and analysis of different rotor structures of double-stator permanent magnet synchronous motor. IET Electric Power Applications; 16: 685–700.

11. Yamakawa T, Wakao S, Kondo K, et al. A new flux weakening operation of interior permanent magnet synchronous motors for Railway Vehicle Traction. 2005 European Conference on Power Electronics and Applications 2005. Epub ahead of print 2005. DOI: 10.1109/epe.2005.219524.

12. Bernard N, Dang L, Olivier JC, et al. Design optimization of high-speed PMSM for electric vehicles. 2015 IEEE Vehicle Power and Propulsion Conference (VPPC) 2015. Epub ahead of print 2015. DOI: 10.1109/vppc.2015.7352927.

13. Brando G, Cervone A, Del Pizzo A, et al. Sensorless control of single-inverter dual-motor AC brushless drives. 2017 IEEE International Symposium on Sensorless Control for Electrical Drives (SLED) 2017. Epub ahead of print 2017. DOI: 10.1109/sled.2017.8078449.

14. Haque ME, Rahman MF. Permanent magnet synchronous motor drives: Analysis, modeling and Control. Saarbrücken, Germany: VDM Verlag Dr. Müller, 2009.

15. Shibano Y, Kubota H. Pole position estimation method of IPMSM at low speed without high frequency components injection. 2009 Twenty-Fourth Annual IEEE Applied Power Electronics Conference and Exposition 2009. Epub ahead of print 2009. DOI: 10.1109/apec.2009.4802661.

16. Yoon-Ho Kim, Yoon-Sang Kook. High performance IPMSM drives without rotational position sensors using reduced-order EKF. IEEE Transactions on Energy Conversion; 14: 868–873.

17. Park N-S, Jang M-H, Lee J-S, et al. Performance improvement of a PMSM sensorless control algorithm using a stator resistance error compensator in the low speed region. Journal of Power Electronics; 10: 485–490.

18. Zhang H, Chen Z, Zhang H. Improved rotor position estimation for IPMSM drives in flux-weakening-based optimized synchronous modulation. 2021 24th International Conference on Electrical Machines and Systems (ICEMS) 2021. Epub ahead of print 2021. DOI: 10.23919/icems52562.2021.9634458.

19. Benjak O, Gerling D. Review of position estimation methods for IPMSM drives without a position sensor part I: Nonadaptive methods. The XIX International Conference on Electrical Machines - ICEM 2010 2010. Epub ahead of print 2010. DOI: 10.1109/icelmach.2010.5607978.

20. Benjak O, Gerling D. Review of position estimation methods for IPMSM drives without a position Sensor Part II: Adaptive methods. The XIX International Conference on Electrical Machines - ICEM 2010 2010. Epub ahead of print 2010. DOI: 10.1109/icelmach.2010.5607980.

21 Wang G, Zhang G, Xu D. Practical issues of sensorless control for PMSM drives. Position Sensorless Control Techniques for Permanent Magnet Synchronous Machine Drives; 281–295.

22. Kim T, Lee H-W, Ehsani M. Position sensorless brushless DC Motor/generator drives: Review and future trends. IET Electric Power Applications; 1: 557.

23. Kim T-H, Ehsani M. Sensorless control of the BLDC Motors from near-zero to high speeds. IEEE Transactions on Power Electronics; 19: 1635–1645.

24. Krishnan R. Rotor position estimation and position sensorless control. Permanent Magnet Synchronous and Brushless DC Motor Drives; 423–454.

25.Boldea I, Agarlita SC. The active flux concept for motion-sensorless unified AC Drives: A Review. International Aegean Conference on Electrical Machines and Power Electronics and Electromotion, Joint Conference 2011. Epub ahead of print 2011. DOI: 10.1109/acemp.2011.6490561.

26.Toso F, Carlet PG, Preindl M, et al. Active-flux-based motion-sensorless control of PMSM using moving horizon estimator. 2018 IEEE 9th International Symposium on Sensorless Control for Electrical Drives (SLED) 2018. Epub ahead of print 2018. DOI: 10.1109/sled.2018.8486107.

27. Sagar SV, Joseph KD. Speed estimation algorithms for sensorless control of PMSM. 2013 International Mutli-Conference on Automation, Computing, Communication, Control and Compressed Sensing (iMac4s) 2013. Epub ahead of print 2013. DOI: 10.1109/imac4s.2013.6526396.

28. Boldea I, Paicu MC, Andreescu G-D, et al. “active flux” DTFC-SVM sensorless control of IPMSM. IEEE Transactions on Energy Conversion; 24: 314–322.

29. Shen JX, Zhu ZQ, Howe D. Sensorless flux-weakening control of permanent magnet brushless machines using third-harmonic back-EMF. IEEE International Electric Machines and Drives Conference, 2003 IEMDC’03. DOI: 10.1109/iemdc.2003.1210397.

30. Song Z, Yao W, Lee K. High-precision sensorless control method with fast dynamic response for high-speed PMSM based on discrete-time back-EMF deadbeat observer. 2021 IEEE Energy Conversion Congress and Exposition (ECCE) 2021. Epub ahead of print 2021. DOI: 10.1109/ecce47101.2021.9595135.

31. Tanaka K, Miki I. Position sensorless control of interior permanent magnet synchronous motor using extended electromotive force. Electrical Engineering in Japan; 161: 41–48.

32. Jung-Hyo Lee, T.ae-Woong Kong, Won-Cheol Lee, et al. A new hybrid sensorless method using a back EMF estimator and a current model of permanent magnet synchronous motor. 2008 IEEE Power Electronics Specialists Conference 2008. Epub ahead of print 2008. DOI: 10.1109/pesc.2008.4592625.

33. Aite Driss Y, Yousfi D. PMSM sensorless control using back-emf based position and speed estimation method. 2013 International Renewable and Sustainable Energy Conference (IRSEC) 2013. Epub ahead of print 2013. DOI: 10.1109/irsec.2013.6529696.

34. Kubota H, Shibano Y, Kobayashi T. Compensation of pole position estimation error for sensor-less IPMSM drives with DC link current detection. 2007 7th International Conference on Power Electronics and Drive Systems 2007. Epub ahead of print 2007. DOI: 10.1109/peds.2007.4487671.

35. Honglin Zhou, Mingwei Kuang, Jiandong Wu. A rotor position and speed estimation method for sensorless control of permanent magnetic synchronous motor. 2012 3rd IEEE International Symposium on Power Electronics for Distributed Generation Systems (PEDG) 2012. Epub ahead of print 2012. DOI: 10.1109/pedg.2012.6254003.

36. Elmas, Zelaya-De La Parra H. Application of a full-order Extended Luenberger Observer for a position sensorless operation of a switched reluctance motor drive. IEE Proceedings - Control Theory and Applications; 143: 401–408.

37. Aydeniz MG, Şenol İ. A Luenberger-sliding mode observer with rotor time constant parameter estimation in induction motor drives. Turkish Journal of Electrical Engineering and Computer Sciences 2011. Epub ahead of print 2011. DOI: 10.3906/elk-1004-4.

38. Yousfi D, Halelfadl A, El Kard M. Review and evaluation of some position and speed estimation methods for PMSM sensorless drives. 2009 International Conference on Multimedia Computing and Systems 2009. Epub ahead of print 2009. DOI: 10.1109/mmcs.2009.5256662.

39. Zhao Y, Qiao W, Wu L. An adaptive quasi-sliding-mode observer-based sensorless drive for heavy-duty interior permanent magnet synchronous machines. 2013 Twenty-Eighth Annual IEEE Applied Power Electronics Conference and Exposition (APEC) 2013. Epub ahead of print 2013. DOI: 10.1109/apec.2013.6520299.

40. Zhiqian Chen, Tomita M, Doki S, et al. An extended electromotive force model for sensorless control of Interior Permanent-magnet synchronous motors. IEEE Transactions on Industrial Electronics; 50: 288–295.

41. Ichikawa S, Zhiqian Chen, Tomita M, et al. Sensorless control of an interior permanent magnet synchronous motor on the rotating coordinate using an extended electromotive force. IECON'01 27th Annual Conference of the IEEE Industrial Electronics Society (Cat No37243). DOI: 10.1109/iecon.2001.975538.

42. Medagam PV, Yucelen T, Pourboghrat F. Adaptive SDRE based nonlinear sensorless speed control for PMSM drives. 2009 American Control Conference 2009. Epub ahead of print 2009. DOI: 10.1109/acc.2009.5160104.

43. Asri A, Ishak D, Iqbal S, et al. A speed sensorless field oriented control of parallel-connected dual PMSM. 2011 IEEE International Conference on Control System, Computing and Engineering 2011. Epub ahead of print 2011. DOI: 10.1109/iccsce.2011.6190590.

44. Wei-Hua Li, Zi-Ying Chen, Wen-Ping Cao. Simulation research on optimization of permanent magnet synchronous motor sensorless vector control based on Mras. 2012 International Conference on Wavelet Active Media Technology and Information Processing (ICWAMTIP) 2012. Epub ahead of print 2012. DOI: 10.1109/icwamtip.2012.6413511.

45. Merzoug. Speed estimation using extended filter Kalman for the direct torque controlled Permanent Magnet Synchronous Motor (PMSM). Advances in Motor Torque Control 2011. Epub ahead of print 2011. DOI: 10.5772/21033.

46. Janiszewski D. Extended Kalman filter based speed sensorless PMSM control with load reconstruction. Kalman Filter 2010. Epub ahead of print 2010. DOI: 10.5772/9593.

47. Aishwarya V, Jayanand B. Estimation and control of sensorless brushless DC motor drive using extended Kalman filter. 2016 International Conference on Circuit, Power and Computing Technologies (ICCPCT) 2016. Epub ahead of print 2016. DOI: 10.1109/iccpct.2016.7530343.

48. Qiu M. . Extended Kalman filter application in permanent magnet synchronous motor sensorless control 2021. Epub ahead of print 2021. DOI: 10.32920/ryerson.14656206.

49. Bolognani S, Oboe R, Zigliotto M. Sensorless full-digital PMSM drive with EKF estimation of speed and rotor position. IEEE Transactions on Industrial Electronics; 46: 184–191.

50. Vyncke TJ, Boel RK, Melkebeek JA. On extended Kalman filters with augmented state vectors for the stator flux estimation in SPMSMs. 2010 Twenty-Fifth Annual IEEE Applied Power Electronics Conference and Exposition (APEC) 2010. Epub ahead of print 2010. DOI: 10.1109/apec.2010.5433462.

51. Benchabane F, Titaoui A, Bennis O, et al. Systematic fuzzy sliding mode approach combined with extented Kalman filter for permanent magnet synchronous motor control. 2010 IEEE International Conference on Systems, Man and Cybernetics 2010. Epub ahead of print 2010. DOI: 10.1109/icsmc.2010.5641677.

52. Comnac, Cirstea, Moldoveanu, et al. Sensorless speed and direct torque control of interior permanent magnet synchronous machine based on extended Kalman filter. Proceedings of the IEEE International Symposium on Industrial Electronics ISIE-02 2002. Epub ahead of print 2002. DOI: 10.1109/isie.2002.1025950.

53. Corley MJ, Lorenz RD. Rotor position and velocity estimation for a salient-pole permanent magnet synchronous machine at standstill and high speeds. IEEE Transactions on Industry Applications; 34: 784–789.

54. Dobrucky B, Michalik J, Spanik P, et al. Virtual HF injection method (VHFIM) of rotor position estimation of PMSM under Field Oriented Control. International Symposium on Power Electronics, Electrical Drives, Automation and Motion, 2006 SPEEDAM 2006. DOI: 10.1109/speedam.2006.1649907.

55. Shanshan Wu, Yongdong Li, Xuejin Miao. Comparison of signal injection methods for sensorless control of PMSM at very low speeds. 2007 European Conference on Power Electronics and Applications 2007. Epub ahead of print 2007. DOI: 10.1109/epe.2007.4417540.

56. Xiao D, Foo G, Rahman MF. A new combined adaptive flux observer with HF signal injection for sensorless direct torque and flux control of matrix converter fed IPMSM over a wide speed range. 2010 IEEE Energy Conversion Congress and Exposition 2010. Epub ahead of print 2010. DOI: 10.1109/ecce.2010.5618149.

57. Wang Y, Zhu J, Guo Y, et al. Torque ripples and estimation performance of high frequency signal injection based sensorless PMSM drive strategies. 2010 IEEE Energy Conversion Congress and Exposition 2010. Epub ahead of print 2010. DOI: 10.1109/ecce.2010.5618116.

58. Anping Z, Jian W. Observation method for PMSM rotor position based on high frequency signal injection. 2010 International Conference on Electrical and Control Engineering 2010. Epub ahead of print 2010. DOI: 10.1109/icece.2010.958.

59. Yan Y, Zhu J. Simulation of a direct torque controlled PMSM drive incorporating structural and saturation saliencies. 2006 37th IEEE Power Electronics Specialists Conference 2006. Epub ahead of print 2006. DOI: 10.1109/pesc.2006.1712015.

60. De Belie FML, Sergeant P, Melkebeek JA. A sensorless drive by applying test pulses without affecting the average-current samples. IEEE Transactions on Power Electronics; 25: 875–888.

61. Chaoui H, Gueaieb W, Yagoub MCE. Neural network based speed observer for interior permanent magnet synchronous motor drives. 2009 IEEE Electrical Power & Energy Conference (EPEC) 2009. Epub ahead of print 2009. DOI: 10.1109/epec.2009.5420924.

62. Butt C, Hoque MA, Rahman MA. Simplified fuzzy logic based MTPA speed control of IPMSM Drive. 38th IAS Annual Meeting on Conference Record of the Industry Applications Conference, 2003. DOI: 10.1109/ias.2003.1257546.

63. Febin Daya JL, Subbiah V. Robust control of sensorless permanent magnet synchronous motor drive using Fuzzy Logic. 2010 2nd International Conference on Advanced Computer Control 2010. Epub ahead of print 2010. DOI: 10.1109/icacc.2010.5486774.

64. Urbanski K, Janiszewski D. Position estimation at zero speed for PMSMs using artificial neural networks. Energies; 14: 8134.

65. Iqbal MA, Memon AY. Robust backstepping sensorless speed control of PMSM using cascaded sliding mode and high gain observers. 2019 International Symposium on Recent Advances in Electrical Engineering (RAEE) 2019. Epub ahead of print 2019. DOI: 10.1109/raee.2019.8886948.

66. Lin F-J, Chen S-G, Sun I-F. Adaptive backstepping control of six-phase PMSM using functional link radial basis function network uncertainty observer. Asian Journal of Control; 19: 2255–2269.

67. Rkhissi-Kammoun Y, Ghommam J, Boukhnifer M, et al. Rise-backsteppping feedback control for induction machine in Electric Vehicle Applications. 2015 23rd Mediterranean

Conference on Control and Automation (MED) 2015. Epub ahead of print 2015. DOI: 10.1109/med.2015.7158812.

68. Dhaouadi R, Mohan N, Norum L. Design and implementation of an extended Kalman filter for the state estimation of a permanent magnet synchronous motor. IEEE Transactions on Power Electronics; 6: 491–497.

69. Haykin SS. Kalman filtering and Neural Networks. New York etc: John Wiley & Sons, 2001.

70. Kim P, Huh L. Kalman filter for beginners: With Matlab examples. United States: CreateSpace, 2011.

71. Mohsin O. . Mobile robot localization based on Kalman filter 2000. Epub ahead of print 2000. DOI: 10.15760/etd.1528.

72. Dilys J, Stankevič V, Łuksza K. Implementation of extended Kalman filter with optimized execution time for sensorless control of a PMSM using ARM cortex-M3 microcontroller. Energies; 14: 3491.

73. Rongyun Z, Changfu G, Peicheng S, et al. The permanent magnet synchronous motor sensorless control of electric power steering based on iterative fifth-order Cubature Kalman filter. Journal of Dynamic Systems, Measurement, and Control 2020; 142. Epub ahead of print 2020. DOI: 10.1115/1.4046613.

74. Fuentes E, Kennel R. Sensorless-predictive torque control of the PMSM using a reduced order extended Kalman filter. 2011 Symposium on Sensorless Control for Electrical Drives 2011. Epub ahead of print 2011. DOI: 10.1109/sled.2011.6051556.